Earth and Planetary Science Letters 331–332 (2012) 128–139

Contents lists available at SciVerse ScienceDirect

Earth and Planetary Science Letters

journal homepage: www.elsevier.com/locate/epsl

A sulfidic driver for the end-Ordovician mass extinction

Emma U. Hammarlund [a,b,c,*], Tais W. Dahl [b], David A.T. Harper [d,f], David P.G. Bond [e], Arne T. Nielsen [f], Christian J. Bjerrum [g], Niels H. Schovsbo [h], Hans P. Schönlaub [i], Jan A. Zalasiewicz [j], Donald E. Canfield [b]

[a] Department of Palaeozoology, Swedish Museum of Natural History, Box 50007, SE-104 05 Stockholm, Sweden
[b] Nordic Center for Earth Evolution (NordCEE) and Institute of Biology, University of Southern Denmark, DK-5230 Odense C, Denmark
[c] Department of Geological Sciences, Stockholm University, SE-106 91 Stockholm, Sweden
[d] Department of Earth Sciences, Durham University, Durham DH1 3LE, UK
[e] School of Earth and Environment, University of Leeds, Leeds LS2 9JT, UK
[f] Natural History Museum of Denmark (Geological Museum), University of Copenhagen, Øster Voldgade 5–7, DK-1350 Copenhagen K, Denmark
[g] Nordic Center for Earth Evolution (NordCEE) and Department of Geography and Geology, University of Copenhagen, Øster Voldgade 10, DK-1350 Copenhagen K, Denmark
[h] Geological Survey of Denmark and Greenland, DK-1350 Copenhagen K, Denmark
[i] Austrian Academy of Science, Center for Geosciences, Vienna, Austria
[j] Department of Geology, University of Leicester, University Road, Leicester, LE1 7RH, UK

ARTICLE INFO

Article history:
Received 26 December 2011
Received in revised form 23 February 2012
Accepted 24 February 2012
Available online xxxx

Editor: J. Lynch-Stieglitz

Keywords:
mass extinction
Ordovician
geochemistry
sulfur

ABSTRACT

The end-Ordovician extinction consisted of two discrete pulses, both linked, in various ways, to glaciation at the South Pole. The first phase, starting just below the *Normalograptus extraordinarius* Zone, particularly affected nektonic and planktonic species, while the second pulse, associated with the *Normalograptus persculptus* Zone, was less selective. Glacially induced cooling and oxygenation are two of many suggested kill mechanisms for the end-Ordovician extinction, but a general consensus is lacking. We have used geochemical redox indicators, such as iron speciation, molybdenum concentrations, pyrite framboid size distribution and sulfur isotopes to analyze the geochemistry in three key Hirnantian sections. These indicators reveal that reducing conditions were occasionally present at all three sites before the first pulse of the end-Ordovician extinction, and that these conditions expanded towards the second pulse. Even though the *N. extraordinarius* Zone appears to have been a time of oxygenated deposition, pyrite is significantly enriched in ^{34}S in our sections as well as in sections reported from South China. This suggests a widespread reduction in marine sulfate concentrations, which we attribute to an increase in pyrite burial during the early Hirnantian. The S-isotope excursion coincides with a major positive carbon isotope excursion indicating elevated rates of organic carbon burial as well. We argue that euxinic conditions prevailed and intensified in the early Hirnantian oceans, and that a concomitant global sea level lowering pushed the chemocline deeper than the depositional setting of our sites. In the *N. persculptus* Zone, an interval associated with a major sea level rise, our redox indicators suggests that euxinic conditions, and ferruginous in some places, encroached onto the continental shelves. In our model, the expansion of euxinic conditions during the *N. extraordinarius* Zone was generated by a reorganization of nutrient cycling during sea level fall, and we argue, overall, that these dynamics in ocean chemistry played an important role for the end-Ordovician mass extinction. During the first pulse of the extinction, euxinia and a steepened oxygen gradient in the water column caused habitat loss for deep-water benthic and nektonic organisms. During the second pulse, the transgression of anoxic water onto the continental shelves caused extinction in shallower habitats.

1. Introduction

The Ordovician Period saw a remarkable rise in marine biodiversity marking the Great Ordovician Biodiversification Event (GOBE) (Droser et al., 1997; Harper, 2006; Sepkoski, 1981; Webby et al., 2004). The biodiversification was, however, punctuated by massive extinction at the end of the Ordovician with an estimated loss of 85% of marine animal species and 26% of animal families (Jablonski, 1991; Sepkoski, 1996; Sheehan, 2001). Two extinction pulses have been documented in some detail (e.g. Brenchley et al., 1994; Fig. 1A). The initial pulse, at the base of, or just below, the *N. extraordinarius* graptolite Zone, is linked to the onset of the end-Ordovician glaciation on the supercontinent Gondwana, then straddling the South Pole (Bergström et al., 2006b; Brenchley, 1984; Brenchley et al., 2001; Finney et al., 2007). However, the timing of glaciation is now debated as recent work indicates that it commenced before the Hirnantian and continued through much of the Silurian (Diaz-Martinez and Grahn, 2007; Finnegan et al., 2011; Nardin et al., 2011). During the first phase of extinction, benthic

* Corresponding author at: Nordic Center for Earth Evolution (NordCEE) and Institute of Biology, University of Southern Denmark, DK-5230 Odense C, Denmark.
E-mail address: emma@biology.sdu.dk (E.U. Hammarlund).

0012-821X/$ – see front matter © 2012 Elsevier B.V. All rights reserved.
doi:10.1016/j.epsl.2012.02.024

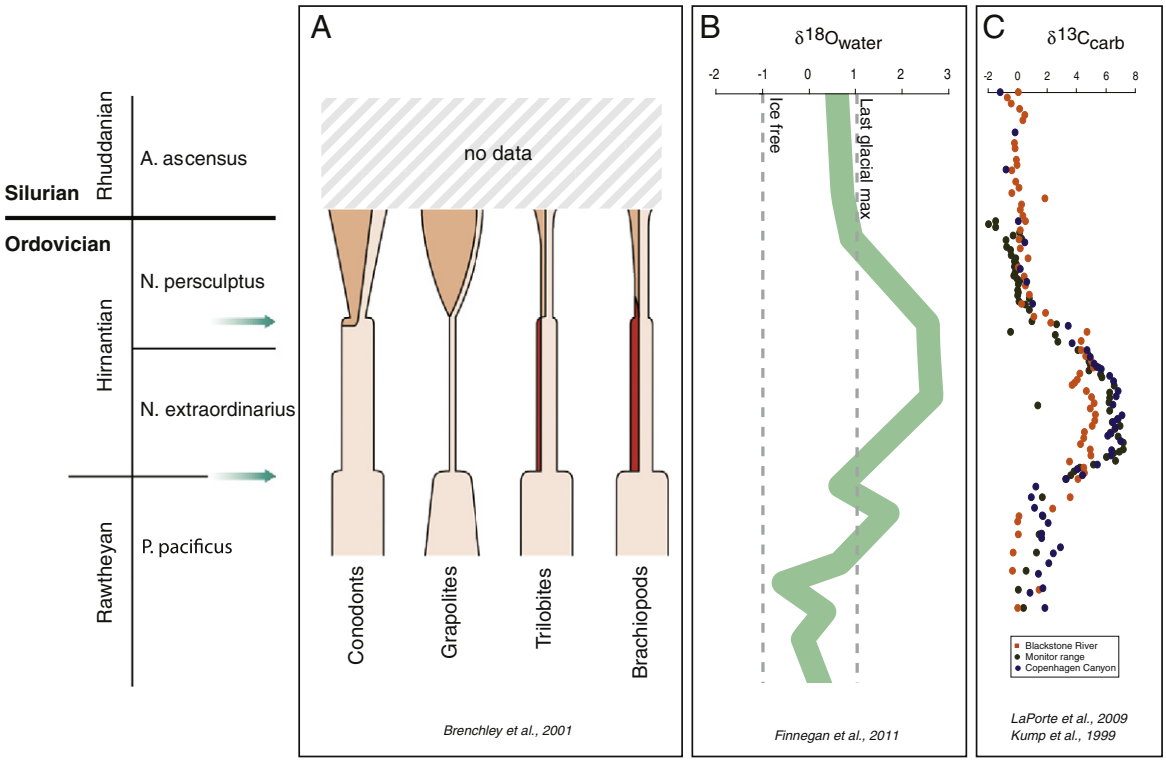

Fig. 1. The end-Ordovician mass extinction (its two phases marked with green arrows), glaciation and carbon excursion. A) Four marine groups affected by the two-phased end-Ordovician extinction (Brenchley et al., 1994). Colors indicate the pre-Hirnantian (beige), Hirnantian (red) and post-Hirnantian (pink) fauna. B) Interpolated $\delta^{18}O$ reflect several fluctuations of the pre-Hirnantian sea level, and a subsequent major drop followed by a rise during the Hirnantian (Finnegan et al., 2011). C) A compilation of three profiles of inorganic $\delta^{13}C$ show a significant perturbation of oceanic carbon dynamics during the early Hirnantian *N. extraordinarius* graptolite Zone (Kump et al., 1999; LaPorte et al., 2009).

organisms in deep and shallow-water environments were more affected than organisms at mid-water depths, and planktonic organisms, particularly graptolites, and nektonic groups, were also hit (see Rasmussen and Harper, 2011a,b). The second pulse of extinction, starting at the base of the *N. persculptus* graptolite Zone, was associated with strong sea level rise (Nielsen, 2004; Fig. 1B). This extinction pulse killed off many survivors from the first crisis, including conodonts, and left simple and cosmopolitan ecosystems behind (Brenchley et al., 2001; Sheehan, 2001).

These extinction pulses occurred during environmental conditions much different from those prevailing today (e.g., Jaanusson, 1984; Servais et al., 2010). Firstly, concentrations of dissolved O_2 in the oceans are inferred to have been, at most, half of modern values, as a result of ambient concentration of O_2 in the atmosphere of 10–50% of present-day levels (PAL) (Bergman et al., 2004; Dahl et al., 2010). Due to these low oxygen levels, inhospitable, anoxic bottom waters would have been common, especially in areas with vigorous nutrient supply and high rates of primary production. Additionally, intense magmatic activity, associated with tectonic rifting and sea floor spreading, is proposed to have resulted in high eustatic sea level stands, extensive epicontinental seas and widespread volcanic eruptions (Barnes, 2004; Haq and Schutter, 2008; Huff et al., 2010; Lefebvre et al., 2010).

A range of potential kill mechanisms have been suggested for the end-Ordovician extinction. The first extinction phase, at the base of, or just below, the *N. extraordinarius* Zone, is commonly linked to rapid cooling and increased oxygenation of the marine water column (Berry et al., 1990; Brenchley et al., 2001; Sheehan, 1988; Skelton, 1994; Stanley, 1988). Increased oxygenation is largely inferred from a widespread shift from the deposition of black shales to the deposition of gray, sometimes bioturbated, shales. The increased oxygenation is then linked to the reduction of habitat for graptolites, possibly living in dysoxic deep-water settings (Wilde and Berry, 1984). In an opposing view, a few studies have discussed how expanded anoxia could be associated with this phase of the extinction. According to this model, the preferential extinction of organisms with at least one pelagic life stage is explained by expansion of water column anoxia (Fortey, 1989). While this idea was forwarded in the absence of any direct geochemical evidence, Chinese and Canadian marine deposits from the early Hirnantian have been interpreted to reflect local, stratified water columns and anoxic conditions at depth (Goodfellow and Jonasson, 1984; Zhang et al., 2009). This interpretation is based on sedimentary pyrite with isotopically heavy sulfur, a phenomenon interpreted to reflect extensive reduction of oceanic sulfate, compatible with anoxic and sulfide-rich conditions. The early Hirnantian also hosts the Hirnantian positive isotopic carbon excursion, the HICE, globally recorded in carbonates (Fig. 1C) that can be taken to indicate increased organic carbon flux to the sea-floor (Bergström et al., 2006b; Brenchley et al., 1994; Finney et al., 1999; see also Kump et al., 1999). Still, these interpretations are at odds with the general impression, based on lithology, that the early Hirnantian was an interval of increased water column oxygenation.

During the second phase of the extinction, anoxia is commonly, inferred based on the widespread deposition of black shales during and following the *N. persculptus* Zone sea level rise (Brenchley et al., 2001; Rong and Harper, 1988). Anoxia has also been argued based on geochemical evidence from mainly South China, where elevated ratios of reactive iron (Fe_{HR}/Fe_T), high trace element abundances as well as isotopically heavy pyrite sulfur can be explained by reducing conditions in a stratified water column (Wang et al., 1993; Yan et al., 2012; Zhang et al., 2009).

Taken together, globally widespread, and direct, evidence of marine redox chemistry dynamics is lacking for the end-Ordovician extinction, and there is no consensus as to what caused, in particular, the first phase of the extinction. In this study, a variety of geochemical paleoredox indicators in three key Hirnantian sections are

investigated (Fig. 2A). We use iron speciation, molybdenum (Mo) concentrations, pyrite framboid size distribution, and the isotopic composition of sulfur (S) and carbon (C) to describe the evolution of ocean chemistry during the two distinctive and contrasting phases of the extinction that led to huge taxonomic losses.

2. Geological settings

2.1. Billegrav, Denmark

The fully cored Billegrav-2 well was drilled on southern Bornholm and extends from the Silurian *Spirograptus turriculatus* Zone in the Rastrites Shale to the Lower Cambrian Rispebjerg Member in the Læså Formation (Schovsbo et al., 2011). The 4.3 m thick Hirnantian section comprises the upper part of the Lindegård Formation and the lowermost part of the Rastrites Shale (Fig. 2A). The Lindegård Formation is a gray, usually bioturbated, mudstone with rare sandstone beds in the upper part, whereas the Rastrites Shale consists of organic-rich, generally non-bioturbated black shale. Graptolite zonation, lithology and gamma-ray log stratigraphy, defined for the nearby Billegrav-1 well, have been used to correlate to the new Billegrav-2 core (cf. Koren' and Bjerreskov, 1997). However, the *Dicellograptus anceps* Zone, immediately prior to the Hirnantian, and the *N. extraordinarius* Zone, in the lower Hirnantian, are devoid of graptolites throughout Baltoscandia. Correlations for this part of the core are therefore mainly inferred based on changes in lithology and composition of the shelly fauna, in combination with the sparse occurrence of chitinozoans (Grahn and Nõlvak, 2010; e.g. Kielan, 1960; Sheehan, 1973). There is, consequently, some uncertainty regarding precisely where the Hirnantian starts in this core, an uncertainty further complicated by the presence of a minor fault within the *N. extraordinarius* Zone.

The rocks have experienced burial temperature of less than 300 °C, as indicated by a 2.3% vitrinite reflectance (Barker and Pawlewicz, 1986; Buchardt et al., 1986). In the Late Ordovician and Early Silurian, the Baltoscandian platform was located in the subtropics around ~30°S (Cocks and Torsvik, 2002). The Hirnantian rocks of Bornholm were deposited in the Tornquist Sea, which was connected to the south-east Iapetus Ocean (Koren' and Bjerreskov, 1997; Fig. 2B). Deposition was occasionally influenced by storms, which suggests that Billegrav is one of the two relatively shallow sites in this study (see Pedersen, 1989). Late Ordovician sedimentation was slow (~4 m/Myr, post-compaction), whereas deposition rates increased during the Silurian (Schovsbo, 2003). The *Dicellograptus* Shale (Sandbian–Katian) contains more than 80 bentonite layers, up to 1 m thick, while no bentonites have been recorded in the Lindegård Formation (upper Katian–Hirnantian) on Bornholm.

2.2. The Carnic Alps, Austria

Outcrop samples were collected in the Cellon avalanche gully, near the Plöcken Pass in the Carnic Alps. The Katian Uggwa Limestone is ~5 m thick and is overlain by the 6.2 m thick Plöcken Formation (Fig. 2A). The Uggwa Limestone consists of wackestones, greenish siltstones and argillaceous lime- to marlstone (Schönlaub et al., 2011). The index graptolite *N. extraordinarius* is not identified in the Carnic Alps, but the upper part of the Uggwa Limestone (Member 2) records the HICE, which has previously been correlated with the *N. extraordinarius* graptolite Zone (Schönlaub et al., 2011). The Plöcken Formation belongs to the *N. persculptus* Zone, and is composed of

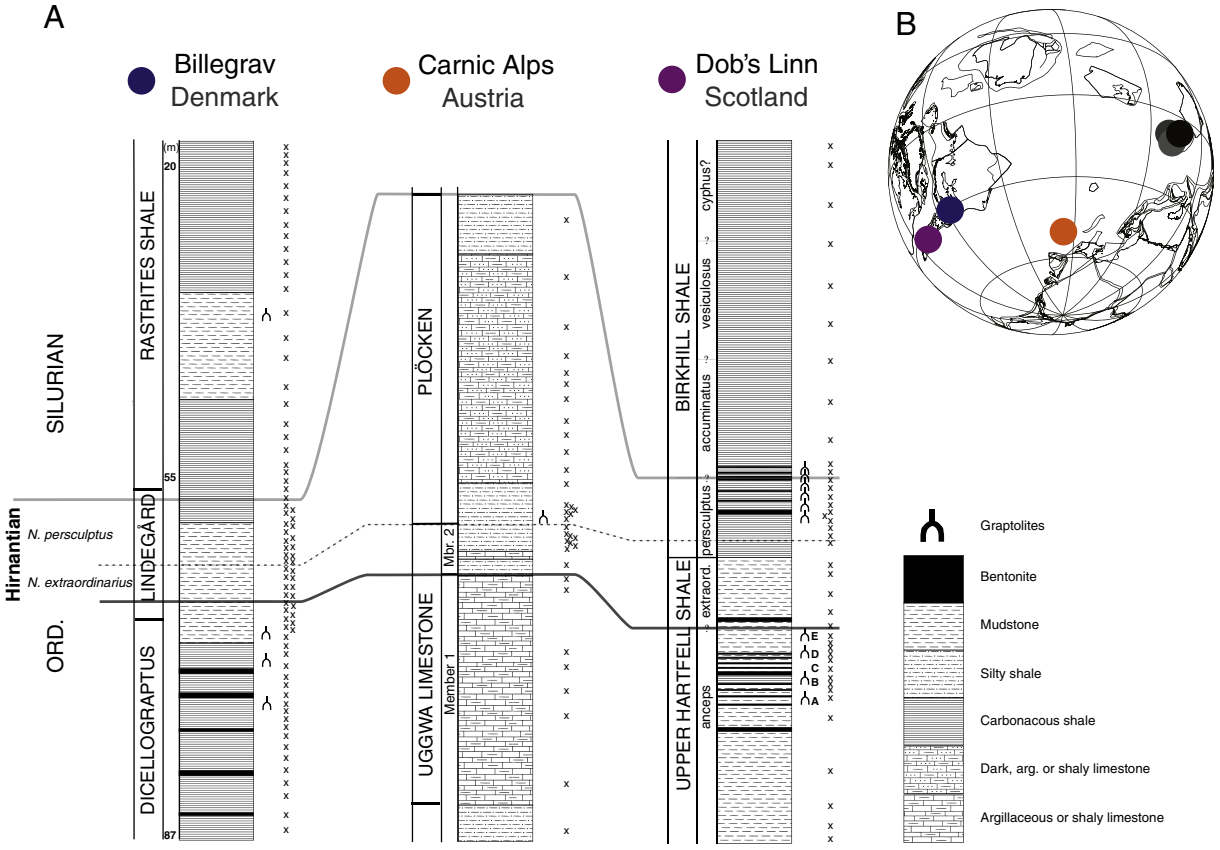

Fig. 2. Stratigraphic and global positions of the studied sample sites. A) Sedimentary logs with sample positions in the Billegrav core, and in the outcrop sections at the Carnic Alps and Dob's Linn. Bentonite occurrences are approximate. *Anceps* Bands at Dob's Linn are marked with a letter next to graptolite symbol. Sample positions marked with X. B) The Hirnantian globe, based on database and reconstruction using the software BugPlates (Torsvik, 2009), showing sample sites for this study: Dob's Linn, UK (purple), Billegrav, Denmark (blue) and the Carnic Alps, Austria (orange) and previously published sections in China (gray-black) (Yan et al., 2009; Zhang et al., 2009).

grayish siltstones with intercalations of limestone lenses (Ferretti and Schönlaub, 2001). Diamictites in parts of the Plöcken Formation record glaciation in this region. In the Carnic Alps, five Hirnantian bentonite horizons of calc-alkaline mafic origin have been identified (Histon et al., 2007). The rocks have experienced a burial temperature of less than 300 °C, based on clay mineralogy and conodont color alteration index (Brime et al., 2008). The sediments were deposited on the shallow slope at the margin of Northern Gondwana, in the Rheic Ocean at ~50°S (Schönlaub, 1993; Schönlaub and Sheehan, 2003; Fig. 2B). The Carnic Alps represent the other shallow-water site in this study.

2.3. Dob's Linn, Scotland

Outcrop samples were collected at Dob's Linn, in the Central Belt of the Southern Uplands terrain (Cocks, 1985; Williams, 1983). Here, the Moffat Shale Group consists of the Upper Hartfell Shale (Katian–early Hirnantian) and the overlying Lower Birkhill Shale (late Hirnantian–Silurian; Fig. 2A). The Upper Hartfell Shale consists of organic-poor, often barren, gray shale interbedded with six organic-rich, laminated bands of graptolitic black shales, the so-called *anceps* Bands (Williams, 1983). The Lower Birkhill Shale is a black, laminated, graptolitic and organic-rich shale, with significant pyrite. The lowermost part of this shale unit belongs to the *N. persculptus* Zone and it also includes the basal Silurian GSSP, dated at 443 ± 1.5 Ma (Ogg et al., 2008). Numerous bentonite horizons (n = 135), of variable thicknesses (1–50 cm), are present (Merriman and Roberts, 1990). The rocks have experienced prehnite–pumpellyite facies metamorphism translating to burial temperatures of ~300 °C (Oliver and Leggett, 1980). Dob's Linn sediments were deposited on the deeper part of the continental slope on the eastern continental margin of Laurentia at ~30°S facing the Iapetus Ocean (Armstrong and Owen, 2002; Cocks and Torsvik, 2002; Kemp and Kelling, 1990; see also Merriman and Roberts, 1990; Fig. 2B). During the Hirnantian, the Iapetus Ocean was in the process of closing, but maintained a connection with the global ocean (Poussart et al., 1999). In this study, we consider Dob's Linn to represent the deepest depositional setting, based on the limited number of benthic organisms preserved and on sedimentological evidence of a low-energy environment. Accumulation rate is estimated at ~4 m/Myr, post-compaction (Wilde et al., 1986).

3. Methods

Iron speciation analyses were performed according to the methods outlined in Poulton and Canfield (2005), and total Fe concentrations were obtained by leaching roasted sediments (8 h at 520 °C) in 6 N HCl for 48 h (Aller et al., 1986). The analytical error for each extraction was less than 5%. The concentrations of the iron species obtained from the chemical extractions were quantified by atomic adsorption spectroscopy (AAS). Pyrite sulfur was extracted by chromium digestion, trapped as Ag_2S, and its concentration determined gravimetrically (Canfield et al., 1986; Zhabina and Volkov, 1978), with a reproducibility of ±5%. Isotopic compositions were determined with a Thermo Analytical elemental analyzer, Flash EA 1112 (sulfur) and EA 2000 (carbon) Series coupled via a ConFlo IV interface to a Thermo Delta V Plus mass spectrometer. S isotope data are reported in terms of per mil difference between $^{34}S/^{32}S$ in the sample and the Vienna Canyon Diablo Troilite (CDT), and C isotope data are reported in terms of per mil difference between $^{13}C/^{12}C$ in the sample and the Vienna Pee Dee Belemnite (V-PDB), with a precision of <0.7‰ (carbon) and <0.3‰ (sulfur). For some of the samples, total organic carbon (TOC) concentrations were measured with the EA Flash 2000 mentioned above, and others in acid-treated sediments (2 N HCl for 2 h), using a Carlo Erba Instruments CHN EA 1108 analyzer within analytical uncertainty of 5%.

Mo concentration analyses were performed in two different labs. At Arizona State University, powdered and roasted (700 °C) marine rocks from Dob's Linn were weighed into Teflon vials and digested using a 5:1 mixture of concentrated HF and HNO_3 for 48 h. After evaporation, the samples were dissolved in 12 N HCl for 24 h, dried, and finally re-dissolved in 6 N HCl. Sample aliquots were dried and re-dissolved in nitric acid before dilution with ultrapure (Milli-Q) water, so that the analyses could be carried out in 2% HNO_3 solutions using a quadropole inductively coupled plasma mass spectrometer ICP-MS (Thermo Elemental X-Series with Collision Cell Technology). Concentrations were obtained by intensity comparison to a multi-element calibration curve, after correction for plasma suppression, using a multi-element internal standard (Ge, In, Y, and Bi) mixed on-line into the sample during analysis. For Mo concentrations, precision is 3%, reproducibility 8% and accuracy is 11% based on comparison with one USGS certified shale reference (SDO-1).

Mo analyses were also performed at the Geological Survey of Denmark and Greenland, where roasted (900 °C) rock powder from Billegrav was digested in a mix of hydrofluoric and nitric acid in closed Teflon vessels on a hotplate at 130 °C for 24 h. Drying and re-dissolving was performed as above, before an internal standard solution (Ge, Rh, and Re) and Milli-Q water was added. The vessels were closed and placed on the hotplate at 130 °C for a minimum of 12 h and then diluted to 50 ml. Mo content was measured using a PerkinElmer Elan 6100DRC ICP-MS instrument with an accuracy of 11% compared to USGS certified shale reference (BHVO-2).

Pyrite framboid size analysis was performed on forty samples from the Ordovician–Silurian interval at Dob's Linn, following the methods detailed in Bond et al. (2004) and Wignall et al. (2010). Samples were examined at the University of Leeds. Where present, pyrite framboid populations (n ≥ 100) were measured. The mean and maximum framboid diameters, as well as the standard deviation, were calculated from the size–frequency distribution.

Where possible, we compare our geochemical data with published data from Chinese sections (Fig. 2B). We correlate biozones as follows (Loydell, 2011): The Ordovician (Katian) zones *P. pacificus* and *D. complexus* in China are binned and correlated to the *D. anceps* Zone in Avalonia. The Silurian (Rhuddanian) *C. vesiculosus* Zone in China corresponds to the *M. acinaces* Zone on Bornholm, while the *C. cyphus* Zone in China is equivalent to the *M. revolutus* Zone on Bornholm. Within each of these bins, sample depths from the different sites are normalized to produce comparable plots. In the plots, each stage, e.g. the Hirnantian Stage (Ordovician) or the Rhuddanian Stage (Silurian), is assigned the same space on the y-axis, while the *N. persculptus* Zone, within the Hirnantian stage, has been given more space (60%) on the y-axis than the *N. extraordinarius* Zone (40%). In the Billegrav core, the oldest samples, from below the *D. complanatus* Zone and underlying the Lindegård Fm, are binned into one unit, and the youngest samples, i.e. post-Rhuddanian (Silurian) are binned together, even though they represent both the Aeronian and the Telychian (Silurian) stages.

4. Results

4.1. Iron

Local water-column redox conditions are evaluated from our Fe speciation results, by quantifying the concentration of iron minerals considered highly reactive (Fe_{HR}) during early sediment diagenesis (Canfield et al., 1992; Poulton et al., 2004). Empirically, it has been shown that ratios of reactive iron over total iron (Fe_{HR}/Fe_T), in modern and ancient sediments, do not exceed 0.38 during normal deposition under an oxic water column (Poulton and Raiswell, 2002; Raiswell and Canfield, 1998). This is a conservative upper value for oxic depositional conditions, as the ratio in oxic sediments is commonly much lower (Poulton and Raiswell, 2002). An anoxic

water column is indicated when the ratio of $Fe_{HR}/Fe_T > 0.38$, and to distinguish whether the water column was characterized by an excess of sulfide over Fe^{2+} (euxinic) or an excess of Fe^{2+} over sulfide (ferruginous), we also evaluate the proportion of the reactive iron that has formed into pyrite (Fe_{PY}/Fe_{HR}). When rocks experience metamorphism above greenschist grade, some iron may be incorporated into unreactive silicate iron phases, resulting in reduced Fe_{HR}/Fe_T values and hence a faulty oxic signal (Raiswell and Canfield, 1998). Likewise, rapid sedimentation dilutes an oxic water-column signal of reactive iron (Anderson and Raiswell, 2004). However, none of the rocks in this study contain turbidites or have experienced metamorphism too high to compromise the iron speciation proxy.

Billegrav contains the oldest pre-Hirnantian samples in this study (Ka1–3; *Dicellograptus* shales), and here, Fe_{HR}/Fe_T values are above 0.38 (Fig. 3A), and Fe_{PY}/Fe_{HR} values are high (0.66 ± 0.10, 1 st. dev.) (Fig. 3B). When approaching the Hirnantian, the Fe_{HR}/Fe_T values at Billegrav drop below 0.38, as do sulfidization of the iron (Fe_{PY}/Fe_{HR}). When this happens at Billegrav, Fe_{HR}/Fe_T values are clustered in an intermediate range in the Carnic Alps (0.32 ± 0.06, 1 st. dev.), while scattered at Dob's Linn (0.31 ± 0.18, 1 st. dev.). However, for samples with Fe_{HR}/Fe_T values above 0.38, the degree of sulfidization (Fe_{PY}/Fe_{HR}) is low for both sites.

In the lower Hirnantian *N. extraordinarius* Zone, Fe_{HR}/Fe_T values are close to or below 0.38 at Billegrav (0.30 ± 0.18, 1 st. dev.) and Dob's Linn (0.29 ± 0.08, 1 st. dev.), while just at 0.38 in the Carnic Alps (0.38 ± 0.17, 1 st. dev.). In the upper Hirnantian, all three sites display increasing Fe_{HR}/Fe_T values. The Fe_{HR}/Fe_T values exceed 0.38 throughout the *N. persculptus* Zone in the Carnic Alps (0.56 ± 0.16, 1 st. dev.), while the values are first below and then above 0.38, upcore, at Billegrav (0.37 ± 0.13, 1 st. dev.) and Dob's Linn (0.56 ± 0.30, 1 st. dev.). Late Hirnantian iron enrichments are also associated with increasing sulfidization of the reactive iron, even if sulfidization remains low for all samples in the Carnic Alps, and for some samples at Dob's Linn. The low degree of sulfidization is not linked to a high proportion of iron oxides (SI Fig. 1), and therefore, is not apparently a product of oxidation during weathering. Towards the upper Hirnantian, Fe_{PY}/Fe_{HR} values approach ~0.7 at Billegrav and Dob's Linn. In the Early Silurian, the rocks are enriched in iron at Billegrav and Dob's Linn (Fe_{HR}/Fe_T at both sites 0.48 ± 0.22, 1 st. dev.), with the highest Fe_{PY}/Fe_{HR} values at Billegrav (0.69 ± 0.12, 1 st. dev.), and with lower and more scattered values at Dob's Linn (0.57 ± 0.21, 1 st. dev.).

4.2. Molybdenum

Mo enrichments, above 10–25 ppm, are also consistent with sediment deposition under euxinic water column conditions (Lyons et al., 2009). Distinct Mo enrichments, manifested as values >10 ppm, are

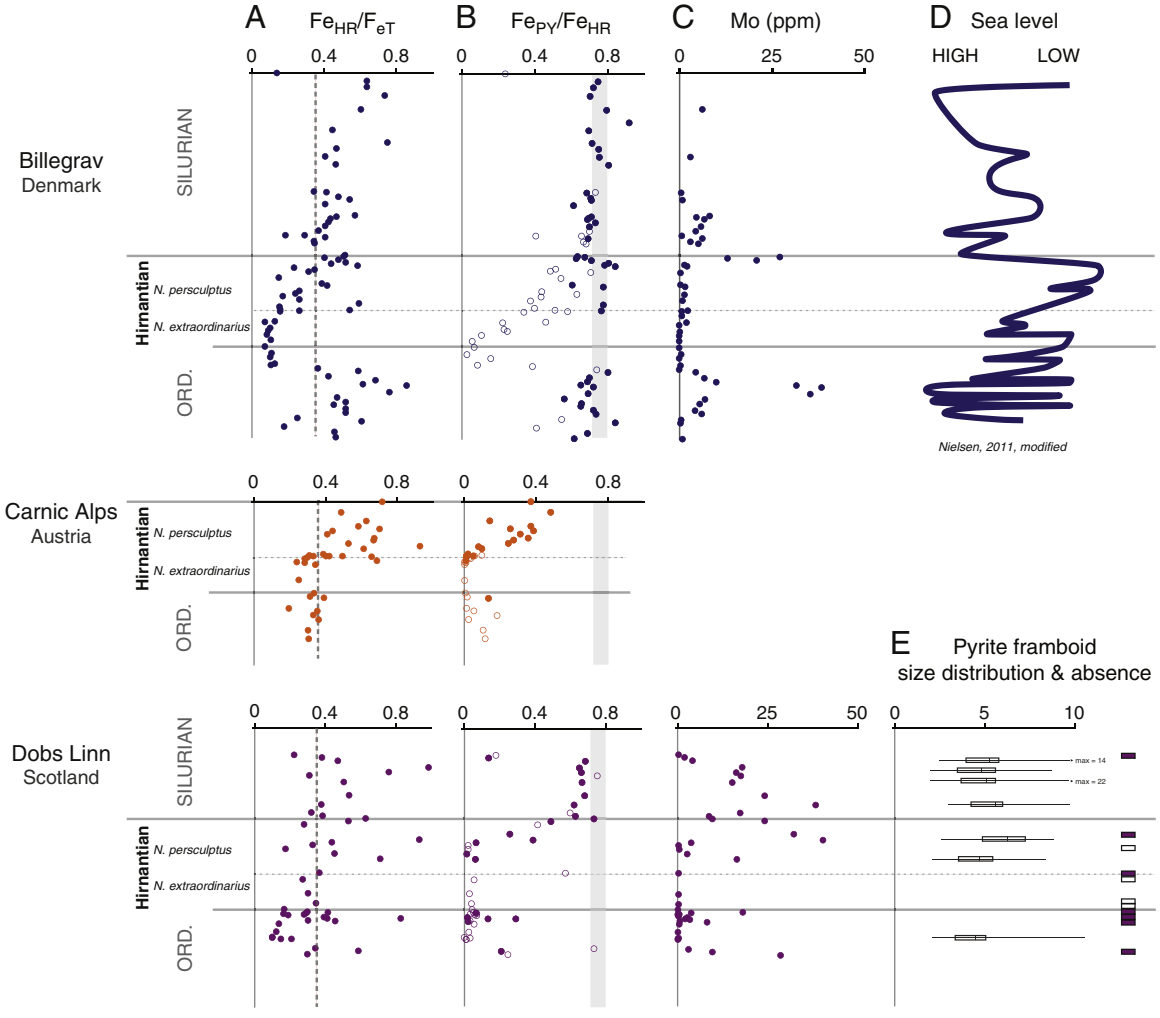

Fig. 3. Iron, molybdenum, sea level and pyrite framboid data for the samples sites reveal extensive euxinic, and occasional ferruginous, conditions. A) Highly reactive iron over total iron (Fe_{HR}/Fe_T), with the threshold at 0.38 (dashed). B) The ratio of pyrite over highly reactive iron (Fe_{PY}/Fe_{HR}), for when Fe_{HR}/Fe_T values are above (filled) and below (open) 0.38. The gray zone indicates the interval which is discussed as a lowermost threshold for euxinic conditions. C) Mo concentrations (ppm) for Dob's Linn and Billegrav. D) Sea level curve for Baltica (Nielsen, 2011, modified). E) Pyrite framboid 'box-and-whisker' plots ($n > 30$). Absence of framboids ($n < 5$) is indicated as small boxes to the right, both when Fe_{HR}/Fe_T is above 0.38 (filled) and below (open). (For interpretation of the references to color in this figure legend, the reader is referred to the web version of this article.)

observed during a short interval in the pre-Hirnantian part of the Billegrav drill core (Ka1–3; *Dicellograptus* shales; Fig. 3C). When approaching the Hirnantian, four samples at Dob's Linn show Mo > 5 ppm. In the lower Hirnantian, Mo concentrations are low at both Billegrav and Dob's Linn (~1 ppm), and close to the crustal average value (~1.5 ppm, Taylor and McLennan, 1995) while >25 ppm Mo are observed towards the end of the Hirnantian. In the Silurian, samples have on average elevated Mo content, higher at Dob's Linn (14.8 ± 10.9, 1 st. dev.) than Billegrav (4.3 ± 2.5, 1 st. dev.).

4.3. Pyrite framboid analysis

Framboids form rapidly in waters supersaturated with respect to both Fe monosulfides and pyrite, and reaction kinetics affect the resulting size distribution (Wilkin et al., 1996). In modern-day euxinic settings, such as the Black Sea, framboids rarely reach 7 μm in diameter before the small particles sink to the sea bed and accumulate as populations with a narrow size distribution (Wilkin et al., 1996). This size–frequency signature provides a valuable criterion for identifying ancient euxinia as it contrasts with the framboid populations formed in sediments underlying oxygenated waters which typically have a broader size distribution and consequently a larger standard deviation (Wilkin and Arthur, 2001; Wilkin et al., 1996). Weathering can oxidize the pyrite to iron oxides, but the framboid size and shape appears unaffected, leaving the pyrite framboids a robust proxy (Bond and Wignall, 2005; Raiswell et al., 2008; Wignall et al., 2010). Therefore, we note the absence of pyrite framboids (n<5) in some of the samples. Their absence, in combination with iron enrichments, could indicate low initial sulfur availability. However, if enough sulfur is available, recent results show that sulfate reduction can occur in an anoxic water column dominated by iron (Crowe et al., 2008). Therefore, one could also suspect that small pyrite framboids are preserved below a ferruginous setting.

Seven samples yielded abundant framboids (n>30), with mean diameters and standard deviations of each population (n≤100) falling within the range indicative of euxinic conditions (Fig. 3E). Only one pre-Hirnantian sample (*anceps* Band B) contained abundant framboids, and this sample showed the smallest mean and lowest standard deviation (average 4.5 μm ± 1.41, 1 st. dev.). No samples in the early Hirnantian yielded pyrite framboids, while six samples from the late Hirnantian and the Early Silurian, contained framboidal pyrite, and these had populations with mean diameters of between 4.7 (±1.4, 1 st. dev.) and 6.3 (±1.6, 1 st. dev.) μm. We also note that five samples from the pre-Hirnantian and early Hirnantian are devoid of framboids (n<5), while Fe_{HR}/Fe_T values are above 0.38, together pointing towards ferruginous conditions.

4.4. Sulfur isotopes

Sedimentary sulfides in pre- and lower-Hirnantian samples from each of our 3 sampling sites exhibit significantly enriched $\delta^{34}S$ compositions (Fig. 4). Indeed, profiles of $\delta^{34}S$ show an excursion in the Hirnantian, which, if measured from its pre-Hirnantian minimum to maximum, ranges, from ~30‰ at Dob's Linn to ~60‰ at Billegrav. Due to the lack of index fossils in the Ashgill–Hirnantian boundary interval of the Billegrav core, the placement of the excursion at Billegrav depends on how the Hirnantian maximum sea level lowstand (sandstone intercalation) is dated. We use a biozone correlation for this site, where the local sandstone interval is interpreted to belong within the *N. persculptus* Zone. With a more conventional placement of the lowstand, in between biozones (at the end of the *N. extraordinarius* Zone), the excursion would be found in the end-Katian (see both correlations in SI Fig. 3). In the Carnic Alps, $\delta^{34}S_{PY}$ values are heavy throughout and no excursion is observed. However, sample resolution in the early Hirnantian of the Carnic Alps is low (n = 3). Our data are correlated with, and plotted next to, $\delta^{34}S_{PY}$ results from three Chinese sections (Yan et al., 2009; Zhang et al., 2009), and all three display a similar isotope excursion. The Chinese sections are generally interpreted to have been deposited in deeper water conditions because of a local drowning of the Yangtze platform earlier in the Late Ordovician (Johnson et al., 1989; Su et al., 2009).

4.5. Organic carbon

TOC concentrations range from 0 to 5 wt.% (average 1.1 ± 1.2 wt.%, 1 st. dev) at Billegrav and from 0 to 4 wt.% (average 0.7 ± 0.9 wt.%, 1 st. dev.) at Dob's Linn (Fig. 5A). Both sections show the highest TOC concentrations in the pre-Hirnantian, followed by a decrease to minimum values at the onset of the Hirnantian. In the upper Hirnantian, TOC concentrations increase at both sites.

The isotopic composition of organic carbon ($\delta^{13}C_{org}$) at Billegrav shows a positive shift of ~4‰ in the Hirnantian, from the pre-Hirnantian baseline (Fig. 5B). $\delta^{13}C_{org}$ returns to lighter values at the end of the Hirnantian. Pre-Hirnantian $\delta^{13}C_{org}$ values from Dob's Linn exhibit a larger range than Billegrav samples of the same age, but a positive $\delta^{13}C_{org}$ excursion, spanning over ~5‰, is apparent at both

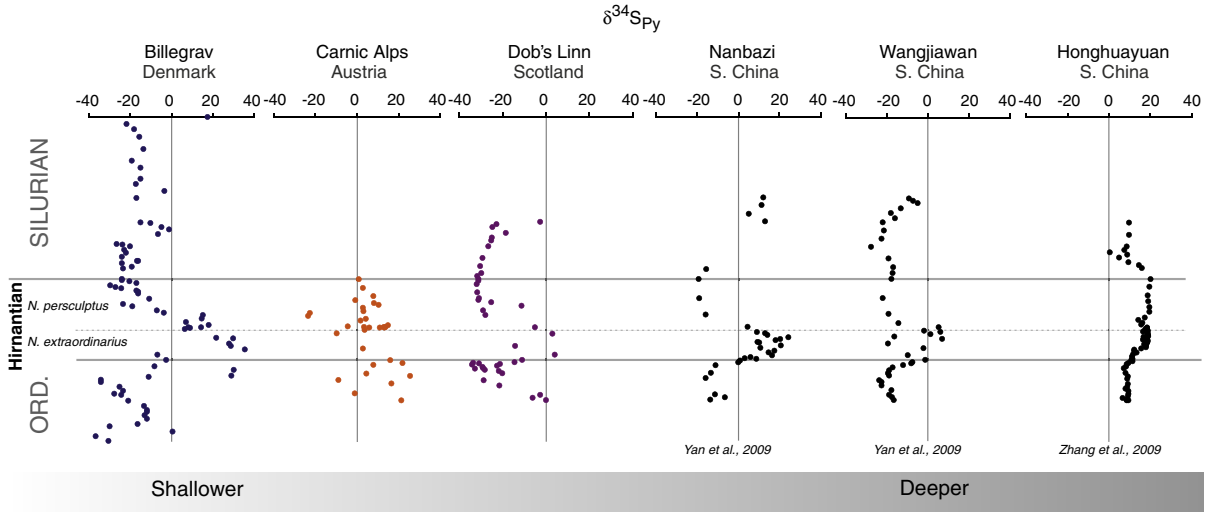

Fig. 4. The $\delta^{34}S$ excursion observed at Billegrav and Dob's Linn, as well as three Chinese sites (Yan et al., 2009; Zhang et al., 2009).

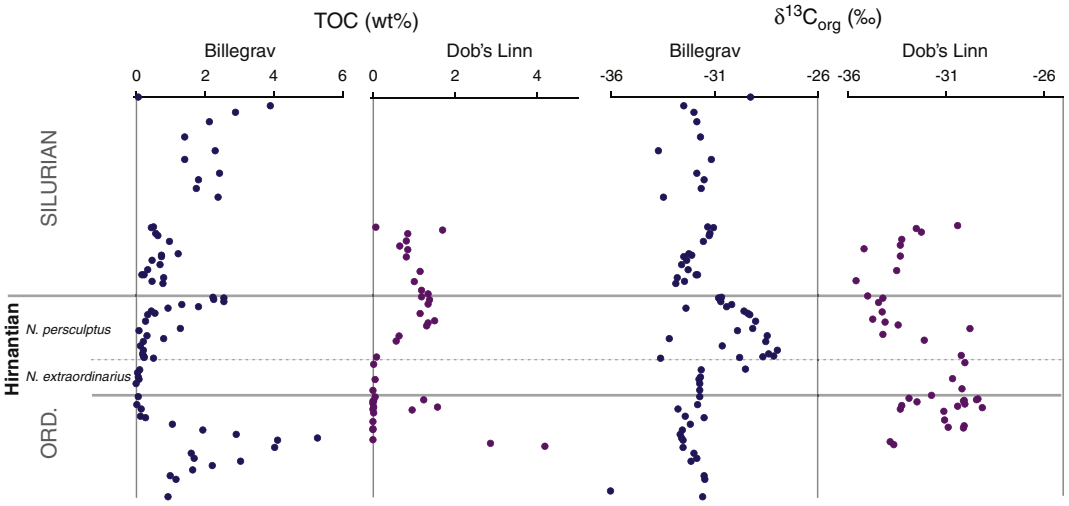

Fig. 5. Total organic carbon (TOC) and the isotopic composition of organic carbon ($\delta^{13}C_{org}$) for Dob's Linn and Billegrav. To better show carbon isotope excursions during the Hirnantian, the scale is designed such that some data points with $\delta^{13}C$ in the range of −36 to −58‰ are not shown. Hence, light samples in Billegrav (3 samples in the pre-Hirnantian) and at Dob's Linn (one pre-Hirnantian sample and two samples in the Early Silurian) are cut off. During the early Hirnantian, the relatively heavy $\delta^{13}C_{org}$ records intense carbon re-cycling while the preserved total organic carbon (TOC) is low.

sites during the Hirnantian. The $\delta^{13}C_{org}$ excursion at Dob's Linn is synchronous with the HICE, while the excursion at Billegrav appears to start a little later. $\delta^{13}C_{org}$ values return to pre-Hirnantian values, at both sites, by the Silurian.

5. Discussion

5.1. Pre-Hirnantian water column chemistry

The oldest deposits analyzed in this study, represented by the bottom-most 12 m of the Billegrav core, show consistent enrichments of highly reactive iron, which we interpret to reflect deposition under an anoxic water column. The iron is furthermore preserved as pyrite at, on average, 70% (±7%, 1 st. dev.). This level of sulfidization could be characteristic of an anoxic water column dominated by sulfide or the upper limit of what is considered deposition under ferruginous conditions (Anderson and Raiswell, 2004; März et al., 2008). However, in this interval, Mo concentrations peak above 25 ppm which is indicative of euxinic conditions (Lyons et al., 2009). Taken together, the evidence points to at least weakly euxinic conditions for a period of ~3 Myr.

Pre-Hirnantian marine deposits from South China add to this picture, as they have recently been interpreted to reveal anoxic conditions (Yan et al., 2012). Also recorded at this point in time is the earliest evidence of the HICE carbon isotope anomaly in various carbonates (see Bergström et al., 2006a; Melchin and Holmden, 2006; Yan et al., 2009). The HICE has been interpreted to reflect a global acceleration of organic carbon burial, during the Hirnantian, and perhaps we see local pre-Hirnantian signs of the same event, through the anoxic waters and the high TOC contents in the earliest part of the Billegrav core, at Dob's Linn as well as in three Chinese sections (Fig. 5A; Yan et al., 2009; Zhang et al., 2009).

Approaching the Hirnantian, we note less evidence of anoxic water column conditions. In the Billegrav core, indications of anoxia (Fe_{HR}/Fe_T, Mo) completely disappear. In the Carnic Alps, iron speciation is clustered around 0.38, which is at the borderline for deposition under modern oxic marine conditions. However, in the Paleozoic, the Fe_{HR}/Fe_T values in oxic marine conditions rarely exceeded 0.20, suggesting the data could represent an anoxic setting (Poulton and Raiswell, 2002). If the Carnic Alp values in fact represent an anoxic depositional setting, sulfidization was low and the water column was hence ferruginous. At Dob's Linn, the Fe_{HR}/Fe_T values are scattered around 0.38, and five of the samples enriched in reactive iron are devoid of pyrite framboids (Fig. 3E, filled boxes), which suggests that sulfide-poor conditions were occasionally present. One graptolitic, black shale *anceps* Band (B) at Dob's Linn is enriched in highly reactive iron, has a low Fe_{PY}/Fe_{HR} value (0.3), modest Mo concentration (<3 ppm) and contains abundant small pyrite framboids. This is also consistent with sulfate reduction in an anoxic water column, even if dominated by iron. These contrasting shifts in pre-Hirnantian water column chemistry are synchronous with the beginning of dramatic sea level changes that affected our sites, as well as the continents globally (Figs. 1B and 3D).

5.2. Early Hirnantian water column chemistry

On average, the global eustatic sea level dropped by 80–150 m during the early Hirnantian (Ghienne et al., 2007; Loi et al., 2010; Nielsen, 2011). In this interval, iron speciation at our study sites indicates a change in water column chemistry. At Billegrav, there was a clear switch to oxic conditions, as suggested by sediment bioturbation and the presence of sparse benthic fauna (trilobites, ostracods). However, while Fe speciation at our sites gives a possible, but equivocal, oxic signal, the early Hirnantian has been viewed by others as a time of overall oxic water column conditions (Berry et al., 1987; Brenchley et al., 1995; Yan et al., 2012; Page et al., 2007). During this interval, we observe an increase in the $\delta^{34}S$ of pyrite by some 30–60‰ compared to the pre-Hirnantian values. A comparable increase is observed in three Chinese sections as well (Fig. 4). Therefore, taken together, this excursion appears geographically widespread. We explore how a global perturbation of the sulfur cycle could have occurred.

Bacterial sulfate reduction (BSR) produces an isotopic fractionation between the sulfate source and the sulfide produced (Canfield, 2001; Kaplan and Rittenberg, 1964). Thus, the isotopic composition of sedimentary sulfides, and seawater sulfate, hold clues to the history of sulfur dynamics in the marine realm (Garrels and Lerman, 1981; Holland, 1973). These dynamics can be described through an isotope mass balance where the isotopic composition of sedimentary pyrite ($\delta^{34}S_{PY}$) is related to the isotopic composition of incoming sulfate ($\delta^{34}S_{IN}$), the fractionation between seawater sulfate and pyrite (Δ), and the fraction of sulfur that

is buried as pyrite (f_{PY}) (remaining sulfur is buried as gypsum, $CaSO_4 \cdot 2\ H_2O$; Eq. (1)).

$$\delta^{34}S_{PY} = \delta^{34}S_{IN} - \Delta(1 - f_{PY}) \quad (1)$$

An increase in $\delta^{34}S_{PY}$ can result either from decreased fractionation (Δ), an increased pyrite burial (f_{PY}), or a change in the $\delta^{34}S_{IN}$. We do not favor an increase in $\delta^{34}S_{IN}$ as an explanation as there is no data to support it, and we cannot reasonably imagine how to generate a necessary increase in this value of the order of 30 to 60‰ (see SI). Instead, the available data, though not abundant, suggest that the isotopic composition of Late Ordovician seawater sulfate ($\delta^{34}S_{SW}$) was not widely variable with a value of ~25‰ (Gill et al., 2007; Kampschulte and Strauss, 2004). Therefore, with the available constraints on $\delta^{34}S_{SW}$, the observed $\delta^{34}S_{PY}$ excursion during the Hirnantian implies a reduction in the fractionation (Δ) between seawater sulfate and pyrite at our three sites from ~45‰ to 20‰ or lower. This fractionation is smaller than typically observed in sediment depositing under oxic conditions today, but such low fractionations can occur when sulfate concentrations become low (Canfield, 2001; Habicht et al., 2002). In the Early Paleozoic, oceanic sulfate concentrations appear to have been low (<8 mM) and a further drop of sulfate concentrations could potentially be reflected in the reduced fractionations we observe (Gill et al., 2007; Horita et al., 2002; Lowenstein et al., 2003).

One way oceanic sulfate concentrations could decrease is through a reduction of sulfur input into the ocean. Sulfate is sourced to the ocean mainly through continental weathering, and the Hirnantian ice sheet may have limited chemical weathering from Gondwana. The magnitude of this effect is hard to gauge, but some weathering would still occur and perhaps even increase, from some rock types, during the glaciation (Gibbs and Kump, 1994). Alternatively, the oceanic sulfate concentrations could have decreased globally as a result of enhanced sulfate removal, most likely as pyrite. We envision that a pulse of expanded euxinic conditions increased the fraction of pyrite burial (f_{PY}) and lowered sulfate concentrations in the ocean, which then led to heavier $\delta^{34}S$ in seawater and in pyrite (Fig. 6B). Expanded water column euxinia and accelerated rates of pyrite burial are also consistent with an increased carbon flux to the sediments, which may be reflected in the concurrent positive carbon excursion observed globally in carbonates, and locally in organic carbon (Figs. 1C and 5B). In combination, the Hirnantian carbon and sulfur isotope records resemble conditions observed during the Late Cambrian SPICE event, when similar perturbations of these cycles have been explained by a marine anoxic event (Gill et al., 2011). Further discussion of this proposed expansion of the water column euxinia during the Hirnantian will be offered below.

Because the isotope composition of seawater sulfate is not well constrained during the Hirnantian, we entertain an alternate hypothesis that the isotopic composition of seawater sulfate dramatically increased during the Hirnantian, driving the increase in $\delta^{34}S_{PY}$ without influencing fractionations. In this scenario, sulfate concentration would have remained high enough to leave fractionations unchanged. As explained above, we do not believe that changes in the $\delta^{34}S$ of river input could have driven such changes in the $\delta^{34}S_{SW}$, but dramatic increases in the pyrite burial could have (Eq. (1)). The driver in both cases would yet be the same, expanded seawater anoxia.

We also explore the possibility that the sulfur isotope excursion arose from diagenetic differences in the Hirnantian versus pre-Hirnantian sedimentary environments. Such an explanation was offered by Yan et al. (2009). Indeed, at Billegrav, light sulfur isotopic compositions of the euxinic interval give way to heavier values in the overlying oxic interval. However, on close inspection, the change to heavy values does not coincide with the switch to oxic deposition (Figs. 3 and 4; SI Fig. 4), so a change in depositional environment is not the immediate cause of the change in isotopic values.

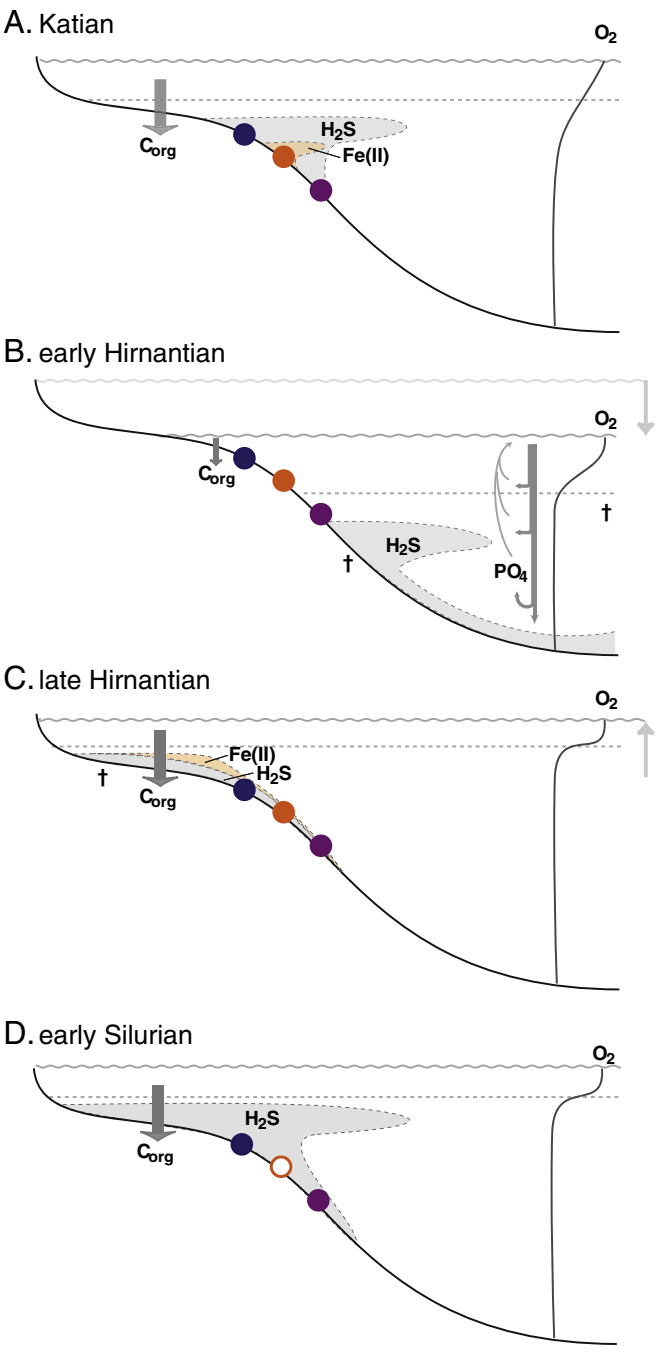

Fig. 6. A conceptual model of the evolution of ocean chemistry prior to, during and after the Hirnantian. (A) Intermittent euxinia were present in the Katian. (B) During the early Hirnantian shelf area was reduced, phosphorus recycling increased and anoxic conditions in the oceans expanded. The fraction of pyrite burial increased and depleted sulfate concentrations. Extinctions (†) occurred among marine animal groups in the water column and at depth. (C) During transgression in the late Hirnantian, sulfate was low and anoxic conditions reached the shelf, affecting shallow benthos. (D) In the Silurian sulfate availability was re-established, resulting in widespread anoxic and sulfidic water column conditions.

Furthermore, sediments from different sections around the world represent a variety of depositional conditions ranging from mildly bioturbated and oxic at Billegrav, un-bioturbated and geochemically equivocal at Dob's Linn and in the Carnic Alps, to varied facies, including black shale, in the Chinese sections (Yan et al., 2009; Zhang et al., 2009). Yet, each section displays a similar shift in the $\delta^{34}S_{PY}$, which we therefore attribute to causes other than changing diagenetic environment.

We are, consequently, left with sulfur and carbon isotope evidence for expanded anoxia at the base of the Hirnantian, despite a move away from obvious signs of euxinic deposition at our study sites. However, we argue that these observations are consistent, and that the eustatic sea level fall taking place at this time forced the euxinic waters below our field of view. Therefore, indications of euxinia disappear at Billegrav and we, at best, get a glimpse of ferruginous water column conditions in the Carnic Alps, and at Dob's Linn (Fig. 6A). The paucity of preserved, deep-water Hirnantian sediments might have bereaved us of direct evidence of euxinia in the geological record, but the isotopic evidence that underlies our interpretation is difficult to explain without invoking extensive euxinia.

5.3. Late Hirnantian water column chemistry

Following the early Hirnantian sea level lowstand, and during the subsequent strong sea level rise, we observe ferruginous conditions consistently in the Carnic Alps and occasionally at Dob's Linn. We argue that the sea level rise reintroduced deep anoxic waters to our three sites (Fig. 6C). That this water was now sulfide-poor is compatible with the previous intense removal of pyrite during the early Hirnantian and a reduction in seawater sulfate availability. During the late Hirnantian, the level of sulfidization then increased gradually at all three sites. This increasing extent of pyritization is geographically widespread, and could reflect a return to somewhat higher oceanic sulfate concentrations. This would suggest that the trigger for expanded anoxia is removed in the mid-Hirnantian. Alternatively, if the ocean was strongly stratified in chemistry, with a ferruginous zone overlying a sulfidic layer (e.g. Li et al., 2010), then our results could reflect, first, the encroachment of ferruginous waters as sea level rose, followed by sulfidic waters, with further sea level rise, as explored immediately below.

Indeed, in the Early Silurian, iron speciation and Mo concentrations reveal consistent sulfide-dominated water columns at Billegrav and at Dob's Linn. The degrees of sulfidization, measured by Fe_{PY}/Fe_{HR} values, indicate weakly sulfidic water column conditions at both sites, which are corroborated by small pyrite framboid size distributions at Dob's Linn. We observe the euxinic conditions during ~2 Myr, represented by the sample set from Dob's Linn, and ~10 Myr, at Billegrav (Fig. 6D).

5.4. Sea level fall as a trigger for anoxia

Growing evidence shows that rapid sea level fall can profoundly affect ocean chemistry, consistent with a scenario of increasing pyrite and organic carbon burial associated with euxinia during end-Ordovician sea level changes. To see how this works, a majority (68%) of marine organic carbon burial takes place in water depths shallower than 200 m (Bjerrum et al., 2006; Lisitzin, 1996). When a sea level drop reduces the shelf area, organic carbon, produced by primary producers, will generally sink through a deep water column adjacent to the continental slopes (Bjerrum et al., 2006; Wallmann, 2003). The longer settling time of organic carbon in the water column leads to a more complete organic carbon decomposition and consequently more efficient recycling of dissolved inorganic phosphate (DIP). Modeling suggests that a sea level drop of 100 m can result in a more than 50% increase in marine DIP concentration, at steady state (Bjerrum and Bendtsen, 2002; Bjerrum et al., 2006; Wallmann, 2003). Because of this, more phosphorus (P) becomes available for primary production. The increased organic matter production then causes enhanced O_2 consumption and drawdown, leading to increased anoxia in the marine water column. During anoxic conditions, enhanced P regeneration from the sediment furthermore creates a positive feedback of P availability (Bjerrum et al., 2006; Tsandev and Slomp, 2009; Van Cappellen and Ingall, 1997).

Referring to this chain of events, we argue that the Hirnantian expansion of anoxic conditions could be driven by the eustatic sea level fall. This is reflected by the coupling of perturbations of both sulfur and the carbon pools, during the Hirnantian, until the trigger for enhanced anoxia disappears after the Hirnantian sea level rise. One question is whether or not the effects of falling sea level could mask the effect of cooling on increased oxygen saturation during this interval. Isotope thermometry has recorded a drop of 5 °C in tropical seawater during the Hirnantian glaciation (Finnegan et al., 2011; Trotter et al., 2008). A temperature drop at high latitudes, where deep water is formed today, say from 5 to 0 °C and with salinity as today, the dissolved O_2 saturation would increase by at most 13%. This increase corresponds to 34 μM at modern pO_2, while at Early Paleozoic pO_2 levels, of 10–50% PAL, surface oxygen levels would at most increase by 17 μM (Bergman et al., 2004; Dahl et al., 2010). Such an increase of dissolved oxygen is small compared to more than ~50 μM minimum reduction of O_2 in deep waters as calculated to accompany a 100 m sea level fall by intensified nutrient recycling, even if the anoxia is already widespread (Fig. 8c of Bjerrum et al., 2006).

Previous hypotheses, and decoupled ocean–atmosphere models, have, however, conveyed the impression that decreased polar temperature, as a result of global cooling and glaciation, would be associated with decreased stratification and increased meridional circulation (Herrmann et al., 2004; Wilde and Berry, 1984). One might think that these effects would reduce, rather than increase, deep water anoxia. There is now growing geochemical evidence, however, that during the last Pleistocene glaciation, deep ocean waters contained less radiocarbon and less oxygen than during the Holocene (Burke and Robinson, 2011; Jaccard and Galbraith, 2011; Lynch-Stieglitz et al., 2007, and references herein). These observations are, in part, thought to be the result of weakened oceanic overturn after changes in the position of the westerly wind maximum as well as variations in the heat and moisture transport in the ocean and atmosphere (de Boer et al., 2007; Olsen et al., 2005; Sigman et al., 2004; Toggweiler and Russell, 2008). Thus, both recent ocean biogeochemical modeling and direct glacial–interglacial observations are consistent with our idea that marine deep ocean anoxia expanded during low sea level of the Hirnantian glaciation.

5.5. Anoxia as kill mechanism

Our conclusion, that marine anoxia expanded during the early Hirnantian, suggests that anoxia may have been a kill mechanism during this first event of animal mass extinction. Expanded euxinia at the base of, or just, below the *N. extraordinarius* Zone would affect marine life in two ways. Euxinia would develop below the mixed layer of the ocean and, in combination with the narrow shelf habitat as a result of eustatic sea level fall, stress the benthic fauna. Anoxia could explain why deep-water benthos, such as the *Foliomena* brachiopod fauna, and trilobites with pelagic larval stages, started to disappear at the end of the Katian (Brenchley et al., 2001; Fortey, 1989; Rasmussen and Harper, 2011a,b). An intensification of water column stratification would also steepen the oxygen gradient, reducing the habitat for the plankton and nekton that hovered in the dysoxic zone as well as exposing them to a higher predation pressure from organisms in the oxic realm (Fig. 6B; Berry et al., 1990). This could account for the biotic turnover observed in the end-Katian, when many graptolites became extinct and phytoplankton communities globally experienced a burst in abundance and morphological variety that could be linked to a changing environment (Finney et al., 2007; Gaucher and Sprechmann, 2009; Vecoli, 2008; Williams, 1983).

It is in fact more difficult to explain the initial pulse of Late Ordovician extinction with kill mechanisms such as oxygenation, loss of continental shelf habitats or cooling. Oxygenation is usually not a

challenge to marine animal life, but instead essential for a range of growth and metabolic processes. Physical habitat loss is no longer the only preferred kill mechanism related to sea level fall. Instead, the pattern of rapid and high-amplitude couplets of regression and transgression have been linked to mass extinctions (Bond and Wignall, 2008; Brenchley, 1984; Hallam and Wignall, 1999; Stanley, 2010). The most cited cause for this extinction phase, cooling, is also problematic. Firstly, the prolonged glacial interval now challenges the hypothesis that the Hirnantian operated fast enough to serve as a direct kill mechanism (Diaz-Martinez and Grahn, 2007; Finnegan et al., 2011; Nardin et al., 2011, and references herein; Stehli and Wells, 1971). There is also a question as to whether the magnitude of the temperature drop associated with the glaciation was sufficient to initiate extinction. In the early Hirnantian tropics, the inferred temperature drop of ~5 °C in shallow water (Finnegan et al., 2011) is comparable to the temperature change of tropical surface seawater during the Pleistocene ice ages, which fell from 28 °C to 25 °C (Herbert et al., 2010). However, the Pleistocene ice ages did not cause marine mass extinctions. Furthermore, Hirnantian deep-water benthic organisms, that went extinct, probably experienced an even smaller temperature shift, if any. Cooling during the Hirnantian was not necessarily lethally sudden or severe for animal life.

Instead, based on the link between sea level fall and water column anoxia, in combination with the data presented in this study, we suggest that anoxia, rather than cooling, was a primary kill mechanism during both phases of the end-Ordovician extinction. During the eustatic sea level rise in the late Hirnantian, the potential increase of habitable shelf area was counterbalanced by euxinic water masses encroaching onto the shelves. This would reduce the number of shallow-water niches and increase competition within them (Valentine, 1969). During this interval of black shale deposition, diversity on the shallow shelf is also reported to be severely diminished (Brenchley et al., 2001).

Finally, we note that perturbations of the global sulfur cycle, in addition to perturbations of the carbon cycle, are now described for all five big mass extinctions, i.e. the Late Devonian (Geldsetzer et al., 1987; Gill et al., 2007; Goodfellow and Jonasson, 1984), the end-Permian (Kajiwara et al., 1994; Newton et al., 2004), the Triassic–Jurassic (Williford et al., 2009), the end-Cretaceous (Kajiwara and Kaiho, 1992) and the end-Ordovician extinction (this study).

6. Conclusions

Local geochemical proxies analyzed in this study, including iron enrichments, Mo concentrations and framboid size distribution indicate that anoxic, even euxinic, conditions were present prior to the Hirnantian at our sample sites Billegrav and Dob's Linn. During the early Hirnantian, we lack direct evidence of ubiquitous anoxia, but observe a globally widespread positive excursion in the $\delta^{34}S$ of pyrite sulfur. We interpret the sulfur excursion to reflect low sulfate concentrations due to an increased sink of sulfur, by elevated rates of pyrite burial. Together with the concurrent global positive carbon isotope excursion, we propose that the early Hirnantian hosted an expansion of euxinic conditions. This scenario is consistent with ocean models of nutrient cycling, and we argue that eustatic sea level fall, apart from bereaving our sample sites of direct evidence for expanding anoxia, triggered the anoxia. In the Ordovician world with low pO_2, this nutrient crisis, driven by sea level fall, muted and overpowered the effects cooling would have on increased solubility of oxygen in the water column. Later in the Hirnantian, reducing conditions are observed at all three study sites, with progressively increasing basinal sulfide levels as sea level rose, implicating a link between anoxia and the second pulse of extinction. Therefore, we argue that water column stratification and anoxia were key kill mechanisms during both phases of the end-Ordovician extinction.

Acknowledgments

We are grateful for the support from Mette Andersen, Brian Harms, Jørgen Kystol, Ariel Anbar, Gwyneth Gordon, Jan Bergström, Annalisa Ferretti, Kathleen Histon, Petr Storch, Micha Ruhl and two anonymous reviewers for helping to shape the ideas presented here. We gratefully acknowledge the financial support from the Danish National Research Foundation, the Swedish Royal Academy of Science, the Carlsberg Foundation, the Villum Kann Rasmussen Foundation and the Danish Council for Independent Research.

Appendix A. Supplementary data

Supplementary data to this article can be found online at doi:10.1016/j.epsl.2012.02.024.

References

Aller, R.C., Mackin, J.E., Cox Jr., R.T., 1986. Diagenesis of Fe and S in Amazon inner shelf muds: apparent dominance of Fe reduction and implications for the genesis of ironstones. Cont. Shelf Res. 6, 263–289.
Anderson, T.F., Raiswell, R., 2004. Sources and mechanisms for the enrichment of highly reactive iron in euxinic Black Sea sediments. Am. J. Sci. 304, 203–233.
Armstrong, H.A., Owen, A.W., 2002. Euconodont paleobiogeography and the closure of the Iapetus Ocean. Geology 30, 1091–1094.
Barker, C.E., Pawlewicz, M.J., 1986. The correlation of vitrinite reflectance with maximum temperature in humic organic matter. In: Buntebarth, G. (Ed.), Paleogeothermics: Evaluation of Geothermal Conditions in the Geological Past: Lecture Notes in Earth Sciences, 5, pp. 79–93.
Barnes, C.R., 2004. Was there an Ordovician superplume event? In: Webby, B.D., Paris, F., Droser, M.L., Percival, I.G. (Eds.), The Great Ordovician Biodiversification Event. Columbia University Press, New York, pp. 77–80.
Bergman, N.M., Lenton, T.M., Watson, A.J., 2004. COPSE: a new model of biogeochemical cycling over Phanerozoic time. Am. J. Sci. 304, 397–437.
Bergström, S.M., Finney, S.C., Xu, C., Goldman, D., Leslie, S.A., 2006a. Three new Ordovician global stage names. Lethaia 39, 287–288.
Bergström, S.M., Saltzman, M.R., Schmitz, B., 2006b. First record of the Hirnantian (Upper Ordovician) delta C-13 excursion in the North American Midcontinent and its regional implications. Geol. Mag. 143, 657–678.
Berry, W.B.N., Wilde, P., Quinby-Hunt, M.S., 1987. The oceanic non-sulfidic oxygen minimum zone: a habitat for graptolites. Bull. Geol. Soc. Den. 35, 103–114.
Berry, W.B.N., Wilde, P., Quinby-Hunt, M., 1990. Late Ordovician Graptolite Mass Mortality and Subsequent early Silurian Re-radiation. Springer Verlag, Berlin.
Bjerrum, C.J., Bendtsen, J., 2002. Relations between long term sea-level change, shelf-ocean exchange and shelf burial of organic material, AGU. Ocean Sciences meeting, Abstract OS41G-08.
Bjerrum, C.J., Bendtsen, J., Legarth, J.J.F., 2006. Modeling organic carbon burial during sea level rise with reference to the Cretaceous. Geochem. Geophys. Geosyst. 7, 1–24.
Bond, D.P.G., Wignall, P.B., 2005. Evidence for Late Devonian (Kellwasser) anoxic events in the Great Basin, western United States. In: Morrow, J., Over, J., Wignall, P.B. (Eds.), Understanding Late Devonian and Permian–Triassic biotic and climatic events: towards an integrated approach. Developments in Palaeontology and Stratigraphy. Elsevier, pp. 225–261.
Bond, D.P.G., Wignall, P.B., 2008. The role of sea-level change and marine anoxia in the Frasnian–Famennian (Late Devonian) mass extinction. Palaeogeogr. Palaeoclimatol. Palaeoecol. 263, 107–118.
Bond, D., Wignall, P.B., Racki, G., 2004. Extent and duration of marine anoxia during the Frasnian–Famennian (Late Devonian) mass extinction in Poland, Germany, Austria and France. Geol. Mag. 141, 173–193.
Brenchley, P.J., 1984. Late Ordovician extinctions and their relationship to the Gondwana glaciation. In: Brenchley, P.J. (Ed.), Fossils and Climate. J. Wiley & Sons, Chichester, pp. 291–316.
Brenchley, P.J., Marshall, J.D., Carden, G.A.F., Robertson, D.B.R., Long, D.G.F., Meidla, T., Hints, L., Anderson, T.F., 1994. Bathymetric and isotopic evidence for a short-lived Late Ordovician glaciation in a greenhouse period. Geology 22, 295–298.
Brenchley, P.J., Carden, G.A.F., Marshall, J.D., 1995. Environmental changes associated with the "first strike" of the late Ordovician mass extinction. Mod. Geol. 20, 69–82.
Brenchley, P.J., Marshall, J.D., Underwood, C.J., 2001. Do all mass extinctions represent an ecological crisis? Evidence from the Late Ordovician. Geol. J. 36, 329–340.
Brime, C., Perri, M.C., Pondrelli, M., Spalletta, C., Venturini, C., 2008. Polyphase metamorphism in the eastern Carnic Alps (N Italy–S Austria): clay minerals and conodont Colour Alteration Index evidence. Int. J. Earth Sci. 97, 1213–1229.
Buchardt, B., Clausen, J., Thomsen, E., 1986. Carbon isotope composition of lower Paleozoic kerogen — effects of maturation. Org. Geochem. 10, 127–134.
Burke, A., Robinson, L.F., 2011. The Southern Ocean's role in carbon exchange during the last deglaciation. Science 335, 557–561.
Canfield, D.E., 2001. Biogeochemistry of sulfur isotopes. In: Valley, J.W., Cole, D.R. (Eds.), Rev. Mineral. Geochem. Mineralogical Society of America, Blacksburg, pp. 607–636.

Canfield, D.E., Raiswell, R., Westrich, J.T., Reaves, C.M., Berner, R.A., 1986. The use of chromium reduction in the analysis of reduced inorganic sulfur in sediments and shales. Chem. Geol. 54, 149–155.
Canfield, D.E., Raiswell, R., Bottrell, S., 1992. The reactivity of sedimentary iron minerals toward sulfide. Am. J. Sci. 292, 659–683.
Cocks, L.R.M., 1985. The Ordovician–Silurian boundary. Episodes 8, 98–100.
Cocks, L.R.M., Torsvik, T.H., 2002. Earth geography from 500 to 400 million years ago: a faunal and palaeomagnetic review. J. Geol. Soc. 159, 631–644.
Crowe, S.A., Jones, C., Katsev, S., Magen, C., O'Neill, A.H., Sturm, A., Canfield, D.E., Haffner, G.D., Mucci, A., Sundby, B., Fowle, D.A., 2008. Photoferrotrophs thrive in an Archean Ocean analogue. Proc. Natl. Acad. Sci. U. S. A. 105, 15938–15943.
Dahl, T.W., Hammarlund, E.U., Anbar, A.D., Bond, D.P.G., Gill, B.C., Gordon, G.W., Knoll, A.H., Nielsen, A.T., Schovsbo, N.H., Canfield, D.E., 2010. Devonian rise in atmospheric oxygen correlated to the radiations of terrestrial plants and large predatory fish. Proc. Natl. Acad. Sci. 107, 17911–17915.
de Boer, A.M., Sigman, D.M., Toggweiler, J.R., Russell, J.L., 2007. Effect of global ocean temperature change on deep ocean ventilation. Paleoceanography 22.
Diaz-Martinez, E., Grahn, Y., 2007. Early Silurian glaciation along the western margin of Gondwana (Peru, Bolivia and northern Argentina): palaeogeographic and geodynamic setting. Palaeogeogr. Palaeoclimatol. Palaeoecol. 245, 62–81.
Droser, M.L., Bottjer, D.J., Sheehan, P.M., 1997. Evaluating the ecological architecture of major events in the Phanerozoic history of marine invertebrate life. Geology 25, 167–170.
Ferretti, A., Schönlaub, H.P., 2001. New conodont faunas from the Late Ordovician of the Central Carnic Alps, Austria. Boll. Soc. Paleontol. Ital. 40, 3–15.
Finnegan, S., Bergmann, K., Eiler, J.M., Jones, D.S., Fike, D.A., Eisenman, I., Hughes, N.C., Tripati, A.K., Fischer, W.W., 2011. The magnitude and duration of Late Ordovician–Early Silurian glaciation. Science 331, 903–906.
Finney, S.C., Berry, W.B.N., Cooper, J.D., Ripperdan, R.L., Sweet, W.C., Jacobson, S.R., Soufiane, A., Achab, A., Noble, P.J., 1999. Late Ordovician mass extinction: a new perspective from stratigraphic sections in central Nevada. Geology 27, 215–218.
Finney, S.C., Berry, W.B.N., Cooper, J.D., 2007. The influence of denitrifying seawater on graptolite extinction and diversification during the Hirnantian (latest Ordovician) mass extinction event. Lethaia 40, 281–291.
Fortey, R.A., 1989. There are extinctions and extinctions — examples from the lower Paleozoic. Philos. Trans. R. Soc. Lond. B Biol. Sci. 325, 327–355.
Garrels, R.M., Lerman, A., 1981. Phanerozoic cycles of sedimentary carbon and sulfur. Proc. Natl. Acad. Sci. U. S. A. 78, 4652–4656.
Gaucher, C., Sprechmann, P., 2009. Chapter 9.1 Neoproterozoic Acritarch Evolution. In: Gaucher, C., Sial, A.N., Frimmel, H.E., Halverson, G.P. (Eds.), Dev. Precambrian Geol., 16, 319–326.
Geldsetzer, H.J., Goodfellow, W.D., McLaren, D.J., Orchard, M.J., 1987. Sulfur-isotope anomaly associated with the Frasnian–Famennian extinction, Medicine Lake, Alberta, Canada. Geology 15, 393–396.
Ghienne, J.F., Boumendjel, K., Paris, F., Videt, B., Racheboeuf, P., Salem, H.A., 2007. The Cambrian–Ordovician succession in the Ougarta Range (western Algeria, North Africa) and interference of the Late Ordovician glaciation on the development of the Lower Palaeozoic transgression on northern Gondwana. Bull. Geosci. 82, 183–214.
Gibbs, M.T., Kump, L.R., 1994. Global chemical erosion during the Last Glacial Maximum and the Present: sensitivity to changes in lithology and hydrology. Paleoceanography 9, 29–543.
Gill, B.C., Lyons, T.W., Saltzman, M.R., 2007. Parallel, high-resolution carbon and sulfur isotope records of the evolving Paleozoic marine sulfur reservoir. Palaeogeogr. Palaeoclimatol. Palaeoecol. 256, 156–173.
Gill, B.C., Lyons, T.W., Young, S.A., Kump, L.R., Knoll, A.H., Saltzman, M.R., 2011. Geochemical evidence for widespread euxinia in the Later Cambrian ocean. Nature 469, 80–83.
Goodfellow, W.D., Jonasson, I.R., 1984. Ocean Stagnation and Ventilation Defined by $\delta^{34}S$ Secular Trends in Pyrite and Barite. Selwyn Basin, Yukon.
Grahn, Y., Nõlvak, J., 2010. Swedish Ordovician Chitinozoa and biostratigraphy: a review and new data. Palaeontographica 283, 1–71.
Habicht, K.S., Gade, M., Thamdrup, B., Berg, P., Canfield, D.E., 2002. Calibration of sulfate levels in the Archean ocean. Science 298, 2372–2374.
Hallam, A., Wignall, P.B., 1999. Mass extinctions and sea-level changes. Earth Sci. Rev. 48, 217–250.
Haq, B.U., Schutter, S.R., 2008. A chronology of Paleozoic sea-level changes. Science 322, 64–68.
Harper, D.A.T., 2006. The Ordovician biodiversification: setting an agenda for marine life. Palaeogeogr. Palaeoclimatol. Palaeoecol. 232, 148–166.
Herbert, T.D., Peterson, L.C., Lawrence, K.T., Liu, Z.H., 2010. Tropical ocean temperatures over the past 3.5 million years. Science 328, 1530–1534.
Herrmann, A.D., Patzkowsky, M.E., Pollard, D., 2004. The impact of paleogeography, pCO_2, poleward ocean heat transport and sea level change on global cooling during the Late Ordovician. Palaeogeogr. Palaeoclimatol. Palaeoecol. 206, 59–74.
Histon, K., Klein, P., Schönlaub, H.P., Huff, W.D., 2007. Lower Paleozoic K-bentonites from the Carnic Alps, Austria. Aust. J. Earth Sci. 100, 26–42.
Holland, H.D., 1973. Systematics of the isotopic composition of sulfur in the oceans during the Phanerozoic and its implications for atmospheric oxygen. Geochim. Cosmochim. Acta 37, 2605–2616.
Horita, J., Zimmermann, H., Holland, H.D., 2002. Chemical evolution of seawater during the Phanerozoic: implications from the record of marine evaporites. Geochim. Cosmochim. Acta 66, 3733–3756.
Huff, W.D., Bergström, S.M., Kolata, D.R., 2010. Ordovician explosive volcanism. Geol. Soc. Am. Spec. Pap. 466, 13–28.
Jaanusson, V., 1984. Ordovician benthic macro-faunal association. In: Bruton, D.L. (Ed.), Aspects of the Ordovician System. Paleont. Contr. Univ, Oslo, pp. 127–139.
Jablonski, D., 1991. Extinctions — a paleontological perspective. Science 253, 754–757.
Jaccard, S.L., Galbraith, E.D., 2011. Large Climate-driven Changes of Oceanic Oxygen Concentrations during the Last Deglaciation. Nature Geosciences advance online publication.
Johnson, M.E., Rong, J., William, F.T., 1989. Comparison of Late Ordovician epicontinental seas and their relative bathymetry in North America and China. Palaios 4, 43–50.
Kajiwara, Y., Kaiho, K., 1992. Oceanic anoxia at the Cretaceous/Tertiary boundary supported by the sulfur isotopic record. Palaeogeogr. Palaeoclimatol. Palaeoecol. 99, 151–162.
Kajiwara, Y., Yamikita, S., Ishida, K., Ishiga, H., Imai, A., 1994. Development of a largely anoxic stratified ocean and its temporary massive mixing at the Permian/Triassic boundary supported by the sulfur isotopic record. Palaeogeogr. Palaeoclimatol. Palaeoecol. 111, 367–379.
Kampschulte, A., Strauss, H., 2004. The sulfur isotopic evolution of Phanerozoic seawater based on the analysis of structurally substituted sulfates in carbonates. Chem. Geol. 204, 255–286.
Kaplan, I.R., Rittenberg, S.C., 1964. Microbiological fractionation of sulphur isotopes. J. Gen. Microbiol. 34, 195–212.
Kemp, A.E.S., Kelling, G., 1990. A field traverse of the Southern Uplands Accretionary Terrane, Scotland. Field Guide 19, International Sedimentological Congress.
Kielan, Z., 1960. Upper Ordovician trilobites from Poland and some related forms from Bohemia and Scandinavia. Palaeontol. Polinica 11, 1–198.
Koren', T., Bjerreskov, M., 1997. Early Llandovery monograptids from Bornholm and the southern Urals: taxonomy and evolution. Bull. Geol. Soc. Den. 44, 1–43.
Kump, L.R., Arthur, M.A., Patzkowsky, M.E., Gibbs, M.T., Pinkus, D.S., Sheehan, P.M., 1999. A weathering hypothesis for glaciation at high atmospheric pCO_2 during the Late Ordovician. Palaeogeogr. Palaeoclimatol. Palaeoecol. 152, 173–187.
LaPorte, D.F., Holmden, C., Patterson, W.P., Loxton, J.D., Melchin, M.J., Mitchell, C.E., Finney, S.C., Sheets, H.D., 2009. Local and global perspectives on carbon and nitrogen cycling during the Hirnantian glaciation. Palaeogeogr. Palaeoclimatol. Palaeoecol. 276, 182–195.
Lefebvre, V., Servais, T., Francois, L., Averbuch, O., 2010. Did a Katian large igneous province trigger the Late Ordovician glaciation? A hypothesis tested with a carbon cycle model. Palaeogeogr. Palaeoclimatol. Palaeoecol. 296, 310–319.
Li, C., Love, G.D., Lyons, T.W., Fike, D.A., Sessions, A.L., Chu, X., 2010. A stratified redox model for the Ediacaran Ocean. Science 328, 80–83.
Lisitzin, A.P., 1996. Oceanic Sedimentation. Lithology and Geochemistry. American Geophysical Union.
Loi, A., Ghienne, J.F., Dabard, M.P., Paris, F., Botquelen, A., Christ, N., Elaouad-Debbaj, Z., Gorini, A., Vidal, M., Videt, B., Destombes, J., 2010. The Late Ordovician glacio-eustatic record from a high-latitude storm-dominated shelf succession: the Bou Ingarf section (Anti-Atlas, Southern Morocco). Palaeogeogr. Palaeoclimatol. Palaeoecol. 296, 332–358.
Lowenstein, T.K., Hardie, L.A., Timofeff, M.N., Demicco, R.V., 2003. Secular variation in seawater chemistry and the origin of calcium chloride basinal brines. Geology 31, 857–860.
Loydell, D.K., 2011. Graptolite biozone correlation charts. Geol. Mag. 1–9.
Lynch-Stieglitz, J., Adkins, J.F., Curry, W.B., Dokken, T., Hall, I.R., Herguera, J.C., Hirschi, J.J.M., Ivanova, E.V., Kissel, C., Marchal, O., Marchitto, T.M., McCave, I.N., McManus, J.F., Mulitza, S., Ninnemann, U., Peeters, F., Yu, E.F., Zahn, R., 2007. Atlantic meridional overturning circulation during the Last Glacial Maximum. Science 316, 66–69.
Lyons, T.W., Anbar, A.D., Severmann, S., Scott, C., Gill, B.C., 2009. Tracking euxinia in the ancient ocean: a multiproxy perspective and proterozoic case study. Annu. Rev. Earth Planet. Sci. 37, 507–534.
März, C., Poulton, S.W., Beckmann, B., Kuster, K., Wagner, T., Kasten, S., 2008. Redox sensitivity of P cycling during marine black shale formation: dynamics of sulfidic and anoxic, non-sulfidic bottom waters. Geochim. Cosmochim. Acta 72, 3703–3717.
Melchin, M.J., Holmden, C., 2006. Carbon isotope chemostratigraphy in Arctic Canada: sea-level forcing of carbonate platform weathering and implications for Hirnantian global correlation. Palaeogeogr. Palaeoclimatol. Palaeoecol. 234, 186–200.
Merriman, R.J., Roberts, B., 1990. Metabentonites in the Moffat Shale Group, Southern Uplands of Scotland — geochemical evidence of ensialic marginal basin volcanism. Geol. Mag. 127, 259–271.
Nardin, E., Godderis, Y., Donnadieu, Y., Le Hir, G., Blakey, R.C., Puceat, E., Aretz, M., 2011. Modeling the early Paleozoic long-term climatic trend. Geol. Soc. Am. Bull. 123, 1181–1192.
Newton, R.J., Pevitt, E.L., Wignall, P.B., Bottrell, S.H., 2004. Large shifts in the isotopic composition of seawater sulphate across the Permo-Triassic boundary in northern Italy. Earth Planet. Sci. Lett. 218, 331–345.
Nielsen, A.T., 2004. Sea-level Changes — A Baltoscandian Perspective. In: Webby, B.D., Droser, M.L., Paris, F., Percival, I.G. (Eds.), The Great Ordovician Biodiversification Event, Part II. Conspectus of the Ordovician World, Columbia, pp. 84–93.
Nielsen, A.T., 2011. A re-calibrated revised sea-level curve for the Ordovician of Baltoscandia. In: Gutiérrez-Marco, J.C., Rábano, I., García-Bellido, D. (Eds.), ISOS — Ordovician of the World, I. Cuadernos del Museo Geominero, Instituto Geológico y Minero de España, Madrid, pp. 399–401.
Ogg, J.G., Ogg, G., Gradstein, F.M., 2008. The Concise Geological Time Scale. Cambridge University Press, New York.
Oliver, G.J.H., Leggett, J.K., 1980. Metamorphism in an accretionary prism: prehnite–pumpellyite facies metamorphism of the Southern Uplands of Scotland. Trans. R. Soc. Edinb. Earth Environ. Sci. 71, 235–246.
Olsen, S.M., Shaffer, G., Bjerrum, C.J., 2005. Ocean oxygen isotope constraints on mechanisms for millennial-scale climate variability. Paleoceanography 20.
Page, A., Zalasiewicz, J., Williams, M., Popov, L.E., 2007. Were transgressive black shales a negative feedback modulating glacioeustacy in the Early Palaeozoic Icehouse.

In: Williams, M., Haywood, A.M., Gregory, F.J., Schmidt, D.N. (Eds.), Deep time perspectives on climate change marrying the signal from computer models and biological proxies. The Micropalaeontological Society, Bath, pp. 123–156.
Pedersen, G.K., 1989. The sedimentology of Lower Palaeozoic black shales from the shallow wells Skelbro 1 and Billegrav 1, Bornholm, Denmark. Bull. Geol. Surv. Denmark 37, 151–173.
Poulton, S.W., Canfield, D.E., 2005. Development of a sequential extraction procedure for iron: implications for iron partitioning in continentally-derived particulates. Chem. Geol. 214, 209–221.
Poulton, S.W., Raiswell, R., 2002. The low-temperature geochemical cycle of iron: from continental fluxes to marine sediment deposition. Am. J. Sci. 302, 774–805.
Poulton, S.W., Krom, M.D., Raiswell, R., 2004. A revised scheme for the reactivity of iron (oxyhydr)oxide minerals towards dissolved sulfide. Geochim. Cosmochim. Acta 68, 3703–3715.
Poussart, P.F., Weaver, A.J., Barnes, C.R., 1999. Late Ordovician glaciation under high atmospheric CO_2: a coupled model analysis. Paleoceanography 14, 542–558.
Raiswell, R., Canfield, D.E., 1998. Sources of iron for pyrite formation in marine sediments. Am. J. Sci. 298, 219–245.
Raiswell, R., Newton, R., Bottrell, S.H., Coburn, P.M., Briggs, D.E.G., Bond, D.P.G., Poulton, S.W., 2008. Turbidite depositional influences on the diagenesis of Beecher's Trilobite Bed and the Hunsruck Slate; sites of soft tissue pyritization. Am. J. Sci. 308, 105–129.
Rasmussen, C.M.Ø., Harper, D.A.T., 2011a. Interrogation of distributional data for the end-Ordovician crisis interval: where did disaster strike? Geol. J. 46, 478–500.
Rasmussen, C.M.Ø., Harper, D.A.T., 2011b. Did the amalgamation of continents drive the end Ordovician mass extinctions? Palaeogeogr. Palaeoclimatol. Palaeoecol. 311, 48–62.
Rong, J.Y., Harper, D.A.T., 1988. The Ordovician–Silurian boundary and the Hirnantian fauna. Lethaia 21 168-168.
Schönlaub, H.P., 1993. Stratigraphy, biogeography and climate relationship of the Alpine Palaeozoic. In: Von Raumer, J.F., Neubauer, F. (Eds.), Pre-Mesozoic Geology in the Alps. Springer, pp. 65–91.
Schönlaub, H.P., Sheehan, P.M., 2003. Die Krise des Lebens am Ende des Ordoviziums. In: Hansch, W. (Ed.), Katastrophen in der Erdgeschichte - Wendezeiten des Lebens, 19. Museo, pp. 82–98.
Schönlaub, H.P., Ferretti, A., Gaggero, L., Hammarlund, E., Harper, D.A.T., Histon, K., Priewalder, H., Spötl, C., Storch, P., 2011. The Late Ordovician glacial event in the Carnic Alps (Austria). In: Gutiérrez-Marco, J.C., Rábano, I., Garcia-Bellido, D. (Eds.), Ordovician of the Worlds. Cuadernos del Museo Geominero, Instituto Geológico y Minero de Espana, Madrid, pp. 515–526.
Schovsbo, N.H., 2003. The geochemistry of Lower Palaeozoic sediments deposited on the margins of Baltica. Bull. Geol. Soc. Den. 50, 11–27.
Schovsbo, N.H., Nielsen, A.T., Klitten, K., Mathiesen, A., Rasmussen, P., 2011. Shale gas investigations in Denmark: lower Palaeozoic shales on Bornholm. Bull. Geol. Surv. Denmark 9–12.
Sepkoski Jr., J.J., 1981. A factor analytic description of the Phanerozoic marine fossil record. Paleobiology 7, 36–53.
Sepkoski, J.J., 1996. Patterns of Phanerozoic extinction: a perspective from global data bases. In: Walliser, O.H. (Ed.), Global Events and Event Stratigraphy in the Phanerozoic. Springer, Berlin, pp. 35–51.
Servais, T., Owen, A.W., Harper, D.A.T., Kroger, B., Munnecke, A., 2010. The Great Ordovician Biodiversification Event (GOBE): the palaeoecological dimension. Palaeogeogr. Palaeoclimatol. Palaeoecol. 294, 99–119.
Sheehan, P.M., 1973. Relation of Late Ordovician glaciation to Ordovician–Silurian changeover in North-American brachiopod faunas. Lethaia 6, 147–154.
Sheehan, P.M., 1988. Late Ordovician events and the terminal Ordovician extinction. Mem. N. Mex. Bur. Mines Miner. Resour. 44, 405–415.
Sheehan, P.M., 2001. The Late Ordovician mass extinction. Annu. Rev. Earth Planet. Sci. 29, 331–364.
Sigman, D.M., Jaccard, S.L., Haug, G.H., 2004. Polar ocean stratification in a cold climate. Nature 428, 59–63.
Skelton, P.W., 1994. Radiations and extinctions in the history of life: what turns the "wheel of fortune"? Eur. Palaeontol. Newsl. 6, 15–21.
Stanley, S.M., 1988. Paleozoic mass extinctions — shared patterns suggest global cooling as a common cause. Am. J. Sci. 288, 334–352.
Stanley, S.M., 2010. Thermal barriers and the fate of perched faunas. Geology 38, 31–34.
Stehli, F.G., Wells, J.W., 1971. Diversity and age patterns in hermatypic corals. Syst. Zool. 20, 115–126.
Su, W.B., Huff, W.D., Ettensohn, F.R., Liu, X.M., Zhang, J.E., Li, Z.M., 2009. K-bentonite, black-shale and flysch successions at the Ordovician–Silurian transition, South China: possible sedimentary responses to the accretion of Cathaysia to the Yangtze Block and its implications for the evolution of Gondwana. Gondwana Res. 15, 111–130.
Taylor, S.R., McLennan, S.M., 1995. The geochemical evolution of the continental crust. Rev. Geophys. 33, 241–265.
Toggweiler, J.R., Russell, J., 2008. Ocean circulation in a warming climate. Nature 451, 286–288.
Torsvik, T.H., 2009. BugPlates: Linking Biogeography and Palaeogeography. www.geodynamics.no.
Trotter, J.A., Williams, I.S., Barnes, C.R., Lecuyer, C., Nicoll, R.S., 2008. Did cooling oceans trigger Ordovician biodiversification? Evidence from conodont thermometry. Science 321, 550–554.
Tsandev, I., Slomp, C.P., 2009. Modeling phosphorus cycling and carbon burial during Cretaceous Oceanic Anoxic Events. Earth Planet. Sci. Lett. 286, 71–79.
Valentine, J.W., 1969. Patterns of taxonomic and ecological structure of the shelf benthos during Phanerozoic time. Palaeontology 12, 684–709.
Van Cappellen, P., Ingall, E.D., 1997. Redox stabilization of the atmosphere and oceans and marine productivity. Science 275, 406–408.
Vecoli, M., 2008. Fossil microphytoplankton dynamics across the Ordovician–Silurian boundary. Rev. Palaeobot. Palynol. 148, 91–107.
Wallmann, K., 2003. Feedbacks between oceanic redox states and marine productivity: a model perspective focused on benthic phosphorus cycling. Glob. Biogeochem. Cycles 17.
Wang, K., Orth, C.J., Attrep, M.J., Chatterton, B.D.E., Wang, X., Li, J., 1993. The great latest Ordovician extinction on the South China Plate: chemostratigraphic studies of the Ordovician–Silurian boundary interval on the Yangtze Platform. Palaeogeogr. Palaeoclimatol. Palaeoecol. 104, 61–79.
Webby, B.D., Droser, M.L., Paris, F., 2004. The Great Ordovician Biodiversification Event (Final Report of IGCP Project 410 (1997–2002)). Columbia University Press.
Wignall, P.B., Bond, D.P.G., Kuwahara, K., Kakuwa, Y., Newton, R.J., Poulton, S.W., 2010. An 80 million year oceanic redox history from Permian to Jurassic pelagic sediments of the Mino-Tamba terrane, SW Japan, and the origin of four mass extinctions. Glob. Planet. Change 71, 109–123.
Wilde, P., Berry, W.B.N., 1984. Destabilization of the oceanic density structure and its significance to marine "extinction" events. Palaeogeogr. Palaeoclimatol. Palaeoecol. 48, 143–162.
Wilde, P., Berry, W.B.N., Quinby-Hunt, M.S., Orth, C.J., Quintana, L.R., Gilmore, J.S., 1986. Iridium abundances across the Ordovician–Silurian stratotype. Science 233, 339–341.
Wilkin, R.T., Arthur, M.A., 2001. Variations in pyrite texture, sulfur isotope composition, and iron systematics in the Black Sea: evidence for Late Pleistocene to Holocene excursions of the O_2–H_2S redox transition. Geochim. Cosmochim. Acta 65, 1399–1416.
Wilkin, R.T., Barnes, H.L., Brantley, S.L., 1996. The size distribution of framboidal pyrite in modern sediments: an indicator of redox conditions. Geochim. Cosmochim. Acta 60, 3897–3912.
Williams, S.H., 1983. The Ordovician–Silurian boundary graptolite fauna of Dob's Linn, Southern Scotland. Palaeontology 26, 605–639.
Williford, K.H., Foriel, J., Ward, P.D., Steig, J., 2009. Major perturbation in sulfur cycling at the Triassic–Jurassic boundary. Geology 37, 835–838.
Yan, D.T., Chen, D.Z., Wang, Q.C., Wang, J.G., Wang, Z.Z., 2009. Carbon and sulfur isotopic anomalies across the Ordovician–Silurian boundary on the Yangtze Platform, South China. Palaeogeogr. Palaeoclimatol. Palaeoecol. 274, 32–39.
Yan, D.T., Chen, D.F., Wang, Q.C., Wang, J.G., 2012. Predominance of stratified anoxic Yangtze Sea interrupted by short-term oxygenation during the Ordo-Silurian transition. Chem. Geol. 291, 69–78.
Zhabina, N.N., Volkov, I.I., 1978. A method of determination of various sulfur compounds in sea sediments and rocks. In: Krumbein, W.E. (Ed.), Environmental Biogeochemistry and Geomicrobiology. Ann Arbor Science Publishers, Ann Arbor, pp. 735–746.
Zhang, T.G., Shen, Y.N., Zhan, R.B., Shen, S.Z., Chen, X., 2009. Large perturbations of the carbon and sulfur cycle associated with the Late Ordovician mass extinction in South China. Geology 37, 299–302.